

Doping tuned anomalous Hall effect in the van der Waals magnetic topological phases $Mn(Sb_{1-x}Bi_x)_4Te_7$

Xin Zhang(张鑫), Zhicheng Jiang(江志诚), Jian Yuan(袁健), Xiaofei Hou(侯骁飞), Xia Wang(王霞),Na Yu(余娜), Zhiqiang Zou(邹志强), Zhengtai Liu(刘正太), Wei Xia(夏威),Zhenhai Yu(于振海), Dawei Shen(沈大伟), and Yanfeng Guo(郭艳峰)

Citation: Chin. Phys. B, 2023, 32 (**9**): 097201. DOI: 10.1088/1674-1056/acd629
Journal homepage: http://cpb.iphy.ac.cn; http://iopscience.iop.org/cpb

What follows is a list of articles you may be interested in

A novel monoclinic phase and electrically tunable magnetism of van der Waals layered magnet $CrTe_2$

Qidi Ren(任启迪), Kang Lai(赖康), Jiahao Chen(陈家浩), Xiaoxiang Yu(余晓翔), and Jiayu Dai(戴佳钰)
Chin. Phys. B, 2023, 32 (**2**): 027201. DOI: 10.1088/1674-1056/ac9b37

Interface-induced topological phase and doping-modulated bandgap of two-dimensioanl graphene-like networks

Ningjing Yang(杨柠境), Hai Yang(杨海), and Guojun Jin(金国钧)
Chin. Phys. B, 2023, 32 (**1**): 017201. DOI: 10.1088/1674-1056/ac904d

Electron delocalization enhances the thermoelectric performance of misfit layer compound $(Sn_{1-x}Bi_xS)_{1.2}(TiS_2)_2$

Xin Zhao(赵昕), Xuanwei Zhao(赵轩为), Liwei Lin(林黎蔚), Ding Ren(任丁), Bo Liu(刘波), and Ran Ang(昂然)
Chin. Phys. B, 2022, 31 (**11**): 117202. DOI: 10.1088/1674-1056/ac6493

Localization correction to the anomalous Hall effect in amorphous CoFeB thin films

Ding Jin-Jun (丁进军), Wu Shao-Bing (吴少兵), Yang Xiao-Fei (杨晓非), Zhu Tao (朱涛)
Chin. Phys. B, 2015, 24 (**2**): 027201. DOI: 10.1088/1674-1056/24/2/027201

Ferromagnetism, variable range hopping and anomalous Hall effect in epitaxial Co:ZnO thin film

Bai Hong-Liang (白洪亮), He Shu-Min (贺树敏), Xu Tong-Shuai (徐同帅), Liu Guo-Lei (刘国磊), Yan Shi-Shen (颜世申), Zhu Da-Peng (朱大鹏), Dai Zheng-Kun (代正坤), Yang Feng-Fan (杨丰帆), Dai You-Yong (代由勇), Chen Yan-Xue (陈延学), Mei Liang-Mo (梅良模)
Chin. Phys. B, 2012, 21 (**10**): 107201. DOI: 10.1088/1674-1056/21/10/107201

Doping tuned anomalous Hall effect in the van der Waals magnetic topological phases $Mn(Sb_{1-x}Bi_x)_4Te_7$

Xin Zhang(张鑫)[1], Zhicheng Jiang(江志诚)[2], Jian Yuan(袁健)[1], Xiaofei Hou(侯骁飞)[1], Xia Wang(王霞)[3], Na Yu(余娜)[3], Zhiqiang Zou(邹志强)[3], Zhengtai Liu(刘正太)[2,6,†], Wei Xia(夏威)[1,5,‡], Zhenhai Yu(于振海)[1], Dawei Shen(沈大伟)[4], and Yanfeng Guo(郭艳峰)[1,5]

[1] *School of Physical Science and Technology, ShanghaiTech University, Shanghai* 201210, *China*
[2] *State Key Laboratory of Functional Materials for Informatics, Shanghai Institute of Microsystem and Information Technology (SIMIT), Chinese Academy of Sciences, Shanghai* 200050, *China*
[3] *Analytical Instrumentation Center, School of Physical Science and Technology, ShanghaiTech University, Shanghai* 201210, *China*
[4] *National Synchrotron Radiation Laboratory, University of Science and Technology of China, Hefei* 230029, *China*
[5] *ShanghaiTech Laboratory for Topological Physics, ShanghaiTech University, Shanghai* 201210, *China*
[6] *Center of Materials Science and Optoelectronics Engineering, University of Chinese Academy of Sciences, Beijing* 100049, *China*

(Received 23 March 2023; revised manuscript received 8 May 2023; accepted manuscript online 17 May 2023)

The van der Waals (vdW) $MnSb_4Te_7$ is a newly synthesized antiferromagnetic (AFM) topological insulator hosting a robust axion insulator state irrelative to the specific spin structure. However, the intrinsic hole doped character of $MnSb_4Te_7$ makes the Fermi level far away from the Dirac point of about 180 meV, which is unfavorable for the exploration of exotic topological properties such as the quantum anomalous Hall effect (QAHE). To shift up the Fermi level close to the Dirac point, the strategy of partially replacing Sb with Bi as $Mn(Sb_{1-x}Bi_x)_4Te_7$ was tried and the magnetotransport properties, in particular, the anomalous Hall effect, were measured and analyzed. Through the electron doping, the anomalous Hall conductance σ_{AH} changes from negative to positive between $x = 0.3$ and 0.5, indicative of a possible topological transition. Besides, a charge neutrality point (CNP) also appears between $x = 0.6$ and 0.7. The results would be instructive for further understanding the interplay between nontrivial topological states and the magnetism, as well as for the exploration of exotic topological properties.

Keywords: anomalous Hall effect, doping, topological materials

PACS: 72.80.Ga, 75.50.Ee, 75.47.–m, 73.43.Nq **DOI:** 10.1088/1674-1056/acd629

1. Introduction

The quantum anomalous Hall effect (QAHE) has attracted considerable interest in recent years owing to its virtue of dissipationless conduction and hence the potential applications in topological computation and other low-consumption devices. The QAHE was observed for the first time in Cr-doped $(Bi, Sb)_2Te_3$ thin film, but the realization temperature is only at sub-Kelvin temperature range due to the small surface gap and disorders cause by the extrinsic doping.[1] To avoid these problems, intrinsic magnetic topological materials are preferable. The intrinsic magnetic topological phases $MnBi_2Te_4/(Bi_2Te_3)_n$ ($n = 1, 2, 3$) have therefore attracted vast attention in recent several years, which exhibit an array of exotic unconventional topological quantum states such as the QAH insulators, axion insulators and magnetic Weyl semimetals (WSMs).[2–6] The prototype member $MnBi_2Te_4$ is an A-type antiferromagnetic (AFM) topological insulator (TI) by naturally stacking the septuple-layer (Te–Bi–Te–Mn–Te–Bi–Te) via van der Waals (vdW) bonding along the crystallographic c-axis,[7] which exhibits a QAH effect at ~ 1.4 K and could be raised up to 6.5 K through turning the Fermi level E_F exactly into the surface exchange gap via gating.[8] However, the realization of QAHE in $MnBi_2Te_4$ requires external magnetic field to align the spins along the same direction, i.e., the system enters into the ferromagnetic (FM) state. The insertion of nonmagnetic quintuple layers (Te–Bi–Te–Bi–Te) into the adjacent MnTe magnetic double layer has been demonstrated as an effective route favoring the FM interaction, which led to the discovery of other members ($n = 1$, 2, 3) in the $MnBi_2Te_4/(Bi_2Te_3)_n$ family. At present, only $MnBi_8Te_{13}$ ($n = 3$) achieves an FM ground state and shows a clean hybridization gap in the surface state.[9–11] However, the QAHE can only be observed in the $n = 0$ and 1 members up to now. To widely demonstrate the exotic topological properties in $MnBi_2Te_4/(Bi_2Te_3)_n$ and raise the working temperature favoring the technical applications, it is of urgent necessity to explore other analogue materials.

The $MnSb_2Te_4/(Sb_2Te_3)_n$ system is an analogue to the $MnBi_2Te_4/(Bi_2Te_3)_n$ family. At present, only the $n = 0$, 1, 2 members are available and the $n = 2$ member displays fragile FM ground state.[12–14] However, by tuning the Mn–Sb antisite defects, the $MnSb_2Te_4$ can also achieve the FM

†Corresponding author. E-mail: ztliu@mail.sim.ac.cn
‡Corresponding author. E-mail: xiawei2@shanghaitech.edu.cn

© 2023 Chinese Physical Society and IOP Publishing Ltd

state.[15–17] For the $n = 1$ member, it shows an intriguing robust axion insulator state regardless of whether the specific magnetic configuration stays at the A-type AFM state or is an external magnetic field driven spin-polarized states, thus providing an excellent platform for studying the axion insulator physics.[13] In the experiment, $MnSb_4Te_7$ is intrinsically hole doped and the E_F is about 180 meV away from the Dirac point (DP), which therefore behaves as a Weyl semimetal with multiple Weyl nodes in the highest valence bands and lowest conduction bands. Tuning the E_F to be close to DP is necessary to explore QAHE and other exotic topological properties. The previous work showed that substitution Sb for Bi in $MnBi_4Te_7$ can achieve the FM state and modify the carrier densities,[18–20] which is instructive to replace the Sb by using Bi in $MnSb_4Te_7$.

We report herein the single crystal growth of $Mn(Sb_{1-x}Bi_x)_4Te_7$ ($x = 0.3$–0.7) and systematic characterizations of the structure, magnetizations, magnetotransport and electronic band structure properties. It is found that the Sb substitution is not only capable of realizing the FM state, but also significantly tunes the location of the E_F of $MnSb_4Te_7$.

2. Experiment

The $Mn(Sb_{1-x}Bi_x)_4Te_7$ ($x = 0.3$, 0.5, 0.6 and 0.7) single crystals were grown by using the self-flux method. Starting materials of Mn (99.95%), Bi (99.999%), Sb (99.999%) and Te (99.999%) blocks were mixed with a specific molar ratio in an alumina crucible, which was then sealed into a quartz tube in vacuum. The assembly was heated in a furnace up to 700 °C within 10 h and kept at that temperature for 10 h, then cooled down to 625 °C in 10 h and slowly cooled down to target temperatures which are shown in Table S1. The assemblies were taken from the furnace and immediately put into a centrifuge to separate the flux and then black crystals with shining surfaces were left in the crucible.

The crystallographic phase and quality of the crystals were examined on a Bruker D2 advance powder x-ray diffractometer (PXRD) with Cu $K\alpha_1$ ($\lambda = 1.54184$ Å) at 298 K. Both (001) surfaces of the crystals were exfoliated to obtain a flat and shiny surface by using the scotch tape method before the following characterizations. Chemical compositions were measured by using the energy dispersive spectroscopy (EDS) on a Phenom-World BV. Three regions were randomly selected on each crystal for the measurements. The measured Sb contents are summarized in Table S2. It is apparent that the Mn contents are less than the nominal ones possibly due to the intrinsic Mn–Sb antisite defects.

The magnetization measurements were performed in a commercial magnetic property measurement system. The magnetic susceptibility $\chi(T)$ was measured between 2 K and 300 K with the zero-field-cooling (ZFC) and field-cooling (FC) modes. During measurements, a magnetic field $\mu_0 H = 100$ Oe was applied with both $H\|c$ and $H\|ab$. The isothermal magnetization ($M(H)$) was measured within the magnetic field and temperature ranges of ±5 T and 2 K–15 K, respectively. The magnetotransport measurements on the freshly cleaved ab plane of the crystals by using a standard six-probe method were conducted in a physical properties measurement system. During measurements of the longitude magnetoresistivity (ρ_{xx}) and Hall resistivity (ρ_{xy}), the current was applied within the ab plane ($I\|ab$) and the magnetic field was parallel to the c-axis ($H\|c$). Magnetic field dependences of ρ_{xx} and ρ_{xy} were symmetrized by using $\rho_{xx} = [\rho_{xx}(+H) + \rho_{xx}(-H)]/2$ and $\rho_{xy} = [\rho_{xy}(+H) - \rho_{xy}(-H)]/2$, respectively.

3. Results and discussion

Figure 1(a) shows the room temperature PXRD of $Mn(Sb_{1-x}Bi_x)_4Te_7$. The clean diffraction peaks arising from the (001) surface of the crystals demonstrate the high quality of the samples used herein. The positions of the peaks slightly shift with different x values indicated by the dotted line in Fig. S1, implying the change of lattice constants upon Bi substitution.[19] The temperature dependent ρ_{xx} for $x = 0.3$, 0.5, 0.6, 0.7 are presented in Fig. 1(b), which display clear kinks caused by magnetic scattering at about 13 K signifying the AFM transition. The enlarged views of $\chi(T)$ and $\rho_{xx}(T)$ between 2 K and 30 K are presented in Figs. 1(c)–1(f), showing a coincident Nèel temperature T_N determined by the cusps. For $x = 0.3$, an AFM transition occurs at 12.8 K manifested by the cusps in $\chi(T)$ for both $H\|c$ and $H\|ab$. As shown in Figs. S2(a) and 2(b), the spin-flop transition of $M(H)$ curve and the platform of $\rho_{xx}(H)$ at 12 K demonstrate the existence of AFM order. With further cooling, $\chi(T)$ of ZFC and FC data for $H\|c$ show a rise at 11.8 K and a separation at 6 K, suggesting the establishment of FM order and the existence of hysteresis at low temperatures. The hysteresis of $M(H)$ and butterfly-shaped loop of $\rho_{xx}(H)$ data as shown in Figs. S2(a) and 2(b) support further evidence for the FM state. The magnetic transition could be explained by involving the competition between the AFM and FM orders.[21]

As seen in Fig. 1(d), for $x = 0.5$, an AFM transition occurs at 13.1 K manifested by the cusps in $\chi(T)$ for $H\|c$. However, $\chi(T)$ of ZFC and FC data shows a separation at about 11 K upon further cooling, which is larger than that of $x = 0.3$. No plateaus are observed in $M(H)$ and $\rho_{xx}(H)$, as shown in Figs. S3(a) and 3(b), manifesting the absence of AFM order.

While for $x = 0.6$, $\chi(T)$ of ZFC and FC data for $H\|c$ presented in Fig. 1(e) shows a rise at 10 K and a separation at 7 K. A similar situation occurs again for $x = 0.7$. As seen

in Fig. 1(f), $\chi(T)$ exhibits a clear rise and separation between ZFC and FC data at ~ 5 K, suggesting the establishment of FM order as also indicated by the $M(H)$ presented in Fig. S5(a). Seen in Figs. S5(a)–S5(c), the $M(H)$ for $x = 0.7$ displays step-like features above 6 K though clear hysteresis loops are visible, corresponding to the AFM or ferrimagnetic state. With further cooling, the hysteresis area becomes larger and the step-like feature gradually vanishes, suggesting that the FM component gradually becomes dominated below 6 K, consistent with the result as seen in $\chi(T)$. It is also manifested by the $\rho_{xx}(H)$ shown in Fig. S5(b) by the clear butterfly-shaped curve and a clear hysteresis loop without step-like feature by the $M(H)$ shown in Fig. S5(b) at 2 K, which is commonly observed in other FM materials.[22] It should be noticed that $\rho_{xx}(T)$ for $x = 0.7$ display continuous decrease upon cooling down to 17 K and then an upturn with further cooling with a slope change at T_N. This behavior may be attributed to that x of 0.7 which is approaching CNP and the carrier density is very small. Such phenomenon was also observed in $Mn(Bi_{0.74}Sb_{0.26})_2Te_4$.[23]

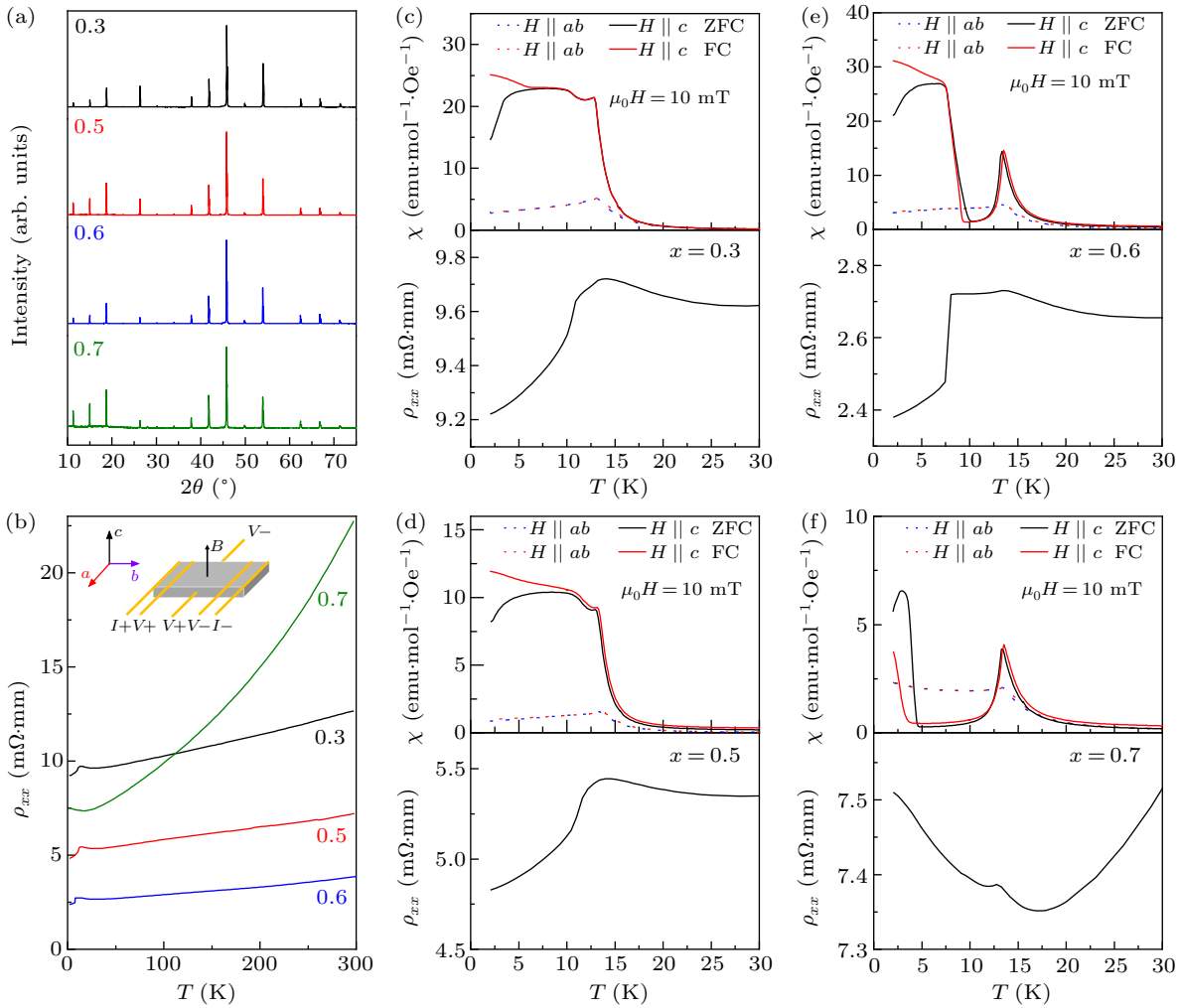


Fig. 1. (a) The PXRD for $Mn(Sb_{1-x}Bi_x)_4Te_7$. (b) The temperature dependence of $\rho_{xx}(T)$ at 2 K–300 K with different x values. (c)–(f) The temperature dependent $\chi(T)$ and ρ_{xx} measured at 2 K–300 K with $x = 0.3$, 0.5, 0.6 and 0.7, respectively. The $\chi(T)$ was measured under $\mu_0 H = 10$ mT between 2 K and 300 K. The blue and red dashed lines represent zero-field cooling (ZFC) and field-cooling (FC) data for $H \| ab$, respectively. The black and red solid lines represent ZFC and FC data for $H \| c$, respectively.

To obtain a clear comparison, the $M(H)$ for $x = 0.3$, 0.4, 0.5, and 0.7 at 2 K are presented together in Fig. 2(a) and also in Fig. 2(b) with enlarged views. It is apparent that all samples show step-like features in the low field range of $\mu_0 H < 0.1$ T, but the $x = 0.3$ and 0.7 show much clearer hysteresis loops than the other two compositions, likely suggesting larger FM components in these two samples. This could also be demonstrated by the clear butterfly-shaped $\rho_{xx}(H)$ curves for $x = 0.3$ and 0.7 at 2 K, seen in Fig. 2(d). As seen in Fig. 2(b) by the isothermal magnetizations, under $\mu_0 H < 0.1$ T, the magnetic field driven spin-polarized states can reach their saturation. It is clear that the saturation moment for $x = 0.5$ is much smaller ($\sim 1\ \mu_B$/Mn) than those of other components, which might be related to the more Mn vacancies and Mn–Sb antisite defects in the sample. As shown in Fig. 2(c), the negative MR ($MR = [\rho_{xx}(H) - \rho_{xx}(0)]/\rho_{xx}(0) \times 100\%$) at the low magnetic field results in the suppression of spin-disorder scattering and the upturn at the high magnetic field for $x = 0.5$

and $x = 0.6$ is caused by the contribution of nonmagnetic $(Sb_{1-x}Bi_x)_2Te_3$.[9,21] In addition, the W shaped *MR* for $x = 0.7$ with positive values at the high magnetic field is due to the large carrier mobility. We have calculated the carrier mobility by using $\mu_H = R_H/\rho_{xx}(0)$, where R_H is the slope of $\rho_{xy}(H)$ and $\rho_{xx}(0)$ is the longitudinal resistivity at zero field. As shown in Fig. 3(c), the results show that the carrier mobility for $x = 0.7$ is about 1527 $cm^2 \cdot V^{-1} \cdot s^{-1}$, which is much larger than those of other samples. Hence, a large positive *MR* is observed, resembling the case in $Mn(Bi_{1-x}Sb_x)_2Te_4$.[24]

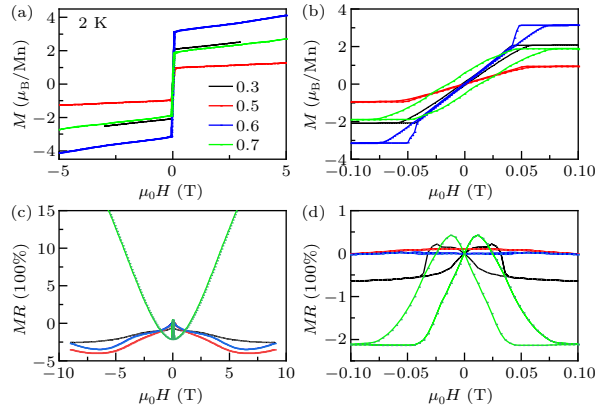


Fig. 2. (a) and (b) Isothermal magnetizations and (c) and (d) magnetoresistance versus magnetic field at 2 K and different magnetic field ranges for $x = 0.3$, 0.4, 0.5 and 0.7.

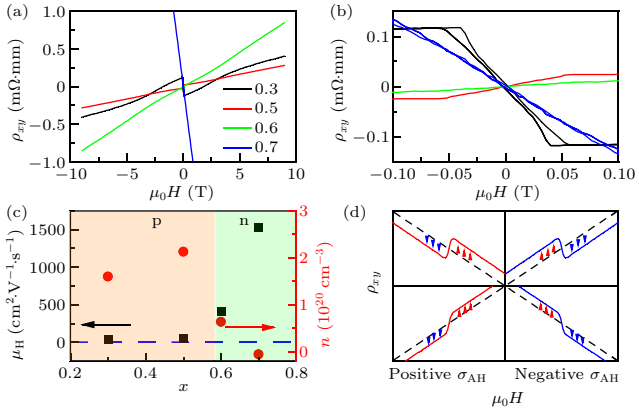


Fig. 3. Evolution of the Hall data for $Mn(Sb_{1-x}Bi_x)_4Te_7$ with $x = 0.3$, 0.4, 0.5, and 0.7 at 2 K. The Hall resistivities are shown under the magnetic field from (a) −9 T to 9 T and (b) −0.1 T to 0.1 T. (c) The carrier mobility and carrier density were extracted from the linear region under the high magnetic field ($\mu_0 H > 5$ T). (d) The Hall resistivity. The left two diagrams represent the positive σ_{AH} and the right two diagrams show the negative σ_{AH}.

The Hall resistivity $\rho_{xy}(H)$ for all doped samples is depicted in Fig. 3(a), showing that the slopes of $\rho_{xy}(H)$ for $x = 0.3$, 0.5 and 0.6 are negative while that for $x = 0.7$ is positive, suggesting the change of carrier type from p- to n-type and a charge neutrality point (CNP) between $x = 0.6$ and 0.7. The result is similar to that of Sb-doped $MnBi_2Te_4$ samples.[18,19] The carrier densities are calculated by using $n = 1/R_H \cdot e$, where the Hall coefficient R_H is the slope of $\rho_{xy}(H)$ and e is the electron charge. Figure 3(c) shows the carrier densities extracted from $\rho_{xy}(H)$ at 2 K within the linear region at $\mu_0 H > 5$ T. The carrier density for $x = 0.7$ is much smaller than that of other samples, indicating that its chemical potential is close to the edge of the conduction or valence band, which is also proved by our ARPES data presented later. Furthermore, we measure another sample (sample 2) of $x = 0.7$ to guarantee the reliability of the result and the same behavior as shown in Fig. S6 is observed, suggesting the intrinsic property of the composition.

The $\rho_{xy}(H)$ for $x = 0.3$ and 0.5 at 2 K both show positive slopes in the high magnetic field region, while displaying significant deviations from the linear field evolution, likely suggesting a multiple band effect. The Hall resistivity $\rho_{xy}(H)$ for $x = 0.3$ shows a negative slope while that of $x = 0.5$ shows a positive slope in the low magnetic field region. The results unveil a reversal of the anomalous Hall conductance σ_{AH}. According to $\sigma_{AH} = e^2 \cdot (-C)/h$, where C is the Chern number. The C value of -1 leads to a positive AHC and $C = +1$ results in a negative AHC,[25] as shown in Fig. 3(d). Considering that the Chern numbers represent different topological states, the reverse sign of σ_{AH} strongly suggests a topological phase transition between $x = 0.3$ and $x = 0.5$.

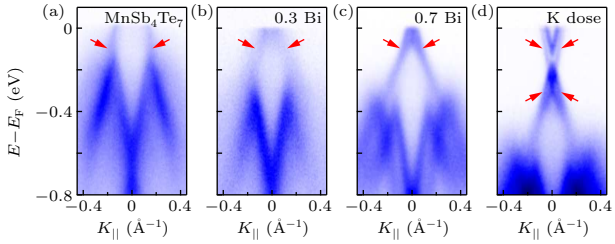


Fig. 4. The ARPES intensity plot taken at 8 K along the $\bar{\Gamma}$–$\bar{K}$ direction for $Mn(Sb_{1-x}Bi_x)_4Te_7$ ($x = 0$, 0.3, 0.7) and K-doped $Mn(Sb_{0.3}Bi_{0.7})_4Te_7$. The red arrows present the topological surface states.

We use the synchrotron-based angle-resolved photoemission spectroscopy (ARPES) to probe the low-energy band structures for $x = 0$, 0.3 and 0.7, with the results shown in Figs. 4(a)–4(c). These ARPES spectra demonstrate the prominent p-type carrier for all samples. For $x = 0$, as studied in our previous work, the E_F is located at $\sim$ 180 meV below the DP.[13] With the substitution of Bi for Sb, the E_F is apparently gradually shifted up, as seen in Figs. 4(b) and 4(c). When $x = 0.7$, the E_F is close to the edge of conduction band, while the DP is invisible yet. With potassium surface doping, the DP is eventually visible by the gapless surface state. The results demonstrate that the $x = 0.7$ is actually close to the CNP in this material. However, it should be noted that, the ARPES data show that the $x = 0.7$ sample is still slightly p-type, which is different from our Hall effect measurement which shows n-type carriers. The discrepancy might be due to that the Hall effect measurements probe the bulk while the ARPES is a surface-sensitive technique and only probes few-layer of the cleaved crystal. Small differences in compositions

can bring large influence on the E_F at the surface, and hence inconsistence of the properties with the bulk. Such phenomenon was also observed in a previous measurement on the analogue system.[24]

4. Conclusion

We grow a series of Bi-doped $MnSb_4Te_7$ crystals and measure the magnetizations, magnetotransport and electronic band structure, which show that the Bi substitution favors the FM exchange and shifts up the Fermi level towards the Dirac point. With the Bi substitution, the Hall resistivity $\rho_{xy}(H)$ changes from positive to negative between $x = 0.6$ and 0.7, and σ_{AH} changes from negative to positive between $x = 0.3$ and 0.5. These behaviors are tightly related to the electronic band structure and provide the opportunity to study the carrier doping induced topological phase transition in $MnSb_4Te_7$. The doping strategy is also instructive for the exploration of exotic topological properties in other magnetic topological phases.

Acknowledgments

Project supported by the Shanghai Science and Technology Innovation Action Plan (Grant No. 21JC1402000), the National Natural Science Foundation of China (Grant No. 12004405), the State Key Laboratory of Functional Materials for Informatics (Grant No. SKL2022), the Double First-Class Initiative Fund of ShanghaiTech University, the Analytical Instrumentation Center (Grant No. SPST-AIC10112914), SPST, and ShanghaiTech University. W. Xia acknowledges the research fund from the State Key Laboratory of Surface Physics and Department of Physics of Fudan University (Grant No. KF2022_13).

References

[1] Chang C Z, Zhang J S, Feng X, Shen J, Zhang Z C, Guo M H, Li K, Ou Y B, Wei P, Wang L L, Ji Z Q, Feng Y, Ji S H, Chen X, Jia J F, Dai X, Fang Z, Zhang S C, He K, Wang Y Y, Lu L, Ma X C and Xue Q K 2013 *Science* **340** 167

[2] Otrokov M M, Menshchikova T V, Vergniory M G, Rusinov I P, Vyazovskaya A Y, Koroteev Y M, Bihlmayer G, Ernst A, Echenique P M, Arnau A and Chulkov E V 2017 *2D Mater.* **4** 025082

[3] Otrokov M M, Rusinov I P, Blanco-Rey M, Hoffmann M, Vyazovskaya A Y, Eremeev S V, Ernst A, Echenique P M, Arnau A and Chulkov E V 2019 *Phys. Rev. Lett.* **122** 107202

[4] Otrokov M M, Klimovskikh I I, Bentmann H, Estyunin D, Zeugner A, Aliev Z S, Gass S, Wolter A U B, Koroleva A V, Shikin A M, Blanco-Rey M, Hoffmann M, Rusinov I P, Vyazovskaya A Y, Eremeev S V, Koroteev Y M, Kuznetsov V M, Freyse F, Sanchez-Barriga J, Amiraslanov I R, Babanly M B, Mamedov N T, Abdullayev N A, Zverev V N, Alfonsov A, Kataev V, Buchner B, Schwier E F, Kumar S, Kimura A, Petaccia L, Di Santo G, Vidal R C, Schatz S, Kissner K, Unzelmann M, Min C H, Moser S, Peixoto T R F, Reinert F, Ernst A, Echenique P M, Isaeva A and Chulkov E V 2019 *Nature* **576** 416

[5] Li J H, Wang C, Zhang Z T, Gu B L, Duan W H and Xu Y 2019 *Phys. Rev. B* **100** 121103

[6] Liu C, Wang Y C, Li H, Wu Y, Li Y X, Li J H, He K, Xu Y, Zhang J S and Wang Y Y 2020 *Nat. Mater.* **19** 522

[7] Gong Y, Guo J W, Li J H, Zhu K J, Liao M H, Liu X Z, Zhang Q H, Gu L, Tang L, Feng X, Zhang D, Li W, Song C L, Wang L L, Yu P, Chen X, Wang Y Y, Yao H, Duan W H, Xu Y, Zhang S C, Ma X C, Xue Q K and He K 2019 *Chin. Phys. Lett.* **36** 076801

[8] Deng Y, Yu Y, Shi M Z, Guo Z, Xu Z, Wang J, Chen X H and Zhang Y 2020 *Science* **367** 895

[9] Hu C W, Ding L, Gordon K N, Ghosh B, Tien H J, Li H X, Linn A G, Lien S W, Huang C Y, Mackey S, Liu J Y, Reddy P V S, Singh B, Agarwal A, Bansil A, Song M, Li D S, Xu S Y, Lin H, Cao H B, Chang T R, Dessau D and Ni N 2020 *Sci. Adv.* **6** eaba4275

[10] Hu C W, Tanatar M A, Prozorov R and Ni N 2022 *J. Phys. D: Appl. Phys.* **55** 054003

[11] Zhong H Y, Bao C H, Wang H, Li J H, Yin Z C, Xu Y, Duan W H, Xia T L and Zhou S Y 2021 *Nano Lett.* **21** 6080

[12] Huan S C, Wang D H, Su H, Wang H Y, Wang X, Yu N, Zou Z Q, Zhang H J and Guo Y F 2021 *Appl. Phys. Lett.* **118** 192105

[13] Huan S C, Zhang S A, Jiang Z C, Su H, Wang H Y, Zhang X, Yang Y C, Liu Z T, Wang X, Yu N, Zou Z Q, Shen D W, Liu J P and Guo Y F 2021 *Phys. Rev. Lett.* **126** 246601

[14] Zhang X, Zhang S, Jiang Z, Huan S, Yang Y, Liu Z, Yang S, Jiao J, Xia W, Wang X, Yu N, Zou Z, Liu Y, Ma J, Shen D, Liu J and Guo Y 2021 arXiv: 2111.04973

[15] Shi G, Zhang M J, Yan D Y, Feng H L, Yang M, Shi Y G and Li Y Q 2020 *Chin. Phys. Lett.* **37** 047301

[16] Ge W B, Sass P M, Yan J Q, Lee S H, Mao Z Q and Wu W D 2021 *Phys. Rev. B* **103** 134403

[17] Yan D Y, Yang M, Song P B, Song Y T, Wang C X, Yi C J and Shi Y G 2021 *Phys. Rev. B* **103** 224412

[18] Chen B, Wang D H, Jiang Z C, Zhang B, Cui S T, Guo J W, Xie H K, Zhang Y, Naveed M, Du Y, Wang X F, Zhang H J, Fei F C, Shen D W, Sun Z and Song F Q 2021 *Phys. Rev. B* **104** 075134

[19] Hu C W, Lien S W, Feng E, Mackey S, Tien H J, Mazin I I, Cao H B, Chang T R and Ni N 2021 *Phys. Rev. B* **104** 054422

[20] Guan Y D, Yan C H, Lee S H, Gui X, Ning W, Ning J L, Zhu Y L, Kothakonda M, Xu C Q, Ke X L, Sun J W, Xie W W, Yang S L and Mao Z Q 2022 *Phys. Rev. Mater.* **6** 054203

[21] Shi M Z, Lei B, Zhu C S, Ma D H, Cui J H, Sun Z L, Ying J J and Chen X H 2019 *Phys. Rev. B* **100** 155144

[22] Yu Z H, Chen X J, Xia W, Wang N N, Lv X, Liu X L, Su H, Li Z Y, Wu D S, Wu W, Liu Z Y, Zhao J G, Li M T, Li S J, Li X, Dong Z H, Zhou C Y, Zhang L L, Wang X, Yu N, Zou Z Q, Luo J L, Cheng J G, Wang L, Zhong Z C and Guo Y F 2022 arXiv: 2202.06016

[23] Yan J Q, Okamoto S, McGuire M A, May A F, McQueeney R J and Sales B C 2019 *Phys. Rev. B* **100** 104409

[24] Lee S H, Graf D, Min L J, Zhu Y L, Yi H M, Ciocys S, Wang Y X, Choi E S, Basnet R, Fereidouni A, Wegner A, Zhao Y F, Verlinde K, He J Y, Redwing R, Gopalan V, Churchill H O H, Lanzara A, Samarth N, Chang C Z, Hu J and Mao Z Q 2021 *Phys. Rev. X* **11** 031032

[25] Moon J, Kim J, Koirala N, Salehi M, Vanderbilt D and Oh S 2019 *Nano Lett.* **19** 3409